Journal of Oral Biosciences 61 (2019) 173–178

Contents lists available at ScienceDirect

Journal of Oral Biosciences

journal homepage: www.elsevier.com/locate/job

Original Article

Comparative assessment of the crystalline structures of powder and bulk human dental enamel by X-ray diffraction analysis

Marjan Behroozibakhsh [a, b, *], Hamidreza Hajizamani [a, b], Kiana Shekofteh [a, b], Mansooreh Otadi [a, c], Mehrsima Ghavami-Lahiji [a, b], Neda Sadat Faal Nazari [d]

[a] Department of Dental Biomaterials, School of Dentistry, Tehran University of Medical Sciences, Tehran, Iran
[b] Research Center for Science and Technology in Medicine, Tehran University of Medical Sciences, Tehran, Iran
[c] Department of Nanomaterial, Faculty of Nanotechnology Campus of Science and Technology, Semnan University, Iran
[d] Sharif University of Technology Central Lab, Iran

ARTICLE INFO

Article history:
Received 15 April 2019
Received in revised form
8 June 2019
Accepted 12 June 2019
Available online 25 June 2019

Keywords:
Crystalline
Dental enamel
X-ray diffraction

ABSTRACT

Objectives: The aim of this study was to assess and compare the crystalline structures of both powder and bulk human dental enamel by X-ray diffraction analysis (XRD).
Methods: The buccal surfaces of 60 selected noncarious third molars were divided into two groups of powdered and bulk enamel specimens. To prepare enamel powders, the enamel tissues were ground and powdered manually using a mortar and pestle. For bulk samples, the enamel slabs were sectioned using a low-speed diamond saw. The crystalline structures of samples were analyzed by XRD, and the obtained data were analyzed. The values of the lattice parameters were obtained using the equation of hexagonal crystalline structures. The crystal sizes and microstrains of crystallites were calculated using both the Scherrer and Williamson–Hall (W–H) methods. The total area under the peaks was considered as the criterion for assessing crystallinity. The data were analyzed by a parametric independent t-test and nonparametric Mann–Whitney test using SPSS for Windows at a significance level of 0.05.
Results: The results of the current study revealed significant differences between the crystallinity values and crystal sizes of the two study groups ($p \leq 0.001$). The powdered samples showed higher crystallinity and smaller crystal sizes than those of the bulk samples. The obtained strain values of the powder samples were nearly twice those of the bulk samples. This difference was not statistically significant ($p = 0.76$).
Conclusions: The results of this study revealed that the sample preparation method for human tooth enamel can affect the crystalline data obtained from XRD analysis.

1. Introduction

Dental enamel is the outmost layer of the tooth structure and is composed of more than 95% minerals by weight [1]. The main structured blocks of enamel are termed prisms and interprisms, and it has been proven that the compositions of both sites are alike and consist of nanosized, fibril-like, hexagonal hydroxyapatite (HAp) crystals. The fundamental difference between the prism and interprism sites is the orientation of HAp crystals, which in the former are parallel to the prism axis and in the latter tend to be inclined perpendicularly to incremental lines [2,3]. The *c*-xis of enamel crystals is orientated preferentially along the long axis of the nanofibrils. The diameter of the nanofibrils is approximately 30–40 nm, and these nanofibrils aggregate with each other to form thicker fibrils with a diameter of approximately 80–130 nm. The size of the cross section of the prism/interprism structure composed of these fibrils is typically 6–8 μm [2] (Fig. 1).

Crystallographically, the enamel crystals belong to the hexagonal close-packed system. Accordingly, the basic structure of enamel apatitic crystals consists of a hexagonal framework of Ca^{2+} and PO_4^{3-} ions around a column of monovalent anions such as OH^- and F^- [4] (Fig. 2b). Two crystallographically different Ca atoms are defined as Ca I (columnar) and Ca II (screw) according to their locations. In a cross-section view of the unit cell, the monovalent ion is surrounded by a triangle of calcium ions (screw). These Ca II

* Corresponding author. Department of Dental Biomaterials, School of Dentistry, Tehran University of Medical Sciences, Tehran, Iran.
E-mail address: behroozibakhsh@tums.ac.ir (M. Behroozibakhsh).

https://doi.org/10.1016/j.job.2019.06.003
1349-0079/

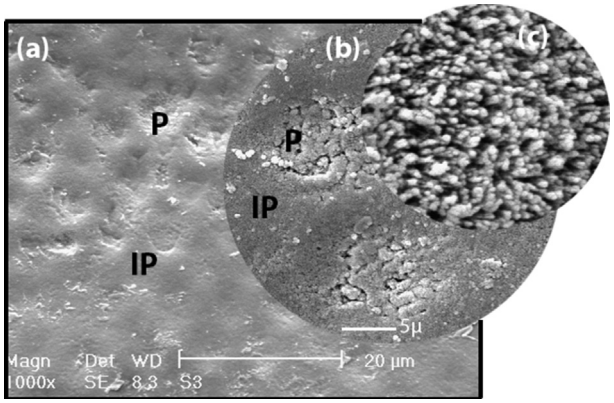

Fig. 1. SEM image of an enamel sample at micro- and nanoscale: (a)–(b) prism/interprism locations with different magnifications; (c) orientation of the enamel fibril-like HAp crystals within the prism at a magnification of x5000.

triangles are surrounded by phosphate ions as well, and the columnar calcium (Ca II) are located hexagonally around the phosphate ions [4,5] (Fig. 2).

The microstructure and biomineralization of dental enamel have always been considered to provide a theoretical basis for the repair of defected enamels and also biomimic synthesis of enamel and novel biomaterials. Previous studies have employed different methods, including scanning electron microscopy (SEM), transmission electron microscopy (TEM), nuclear magnetic resonance spectroscopy, atomic force microscopy, Fourier-transform infrared spectroscopy, and XRD [2,7–10], to reveal the unique microstructures of enamel. As a direct observational technique, TEM has more often been used to evaluate the ultrastructures of materials for all scales down to a resolution of 1 Å [11]. XRD is also a powerful technique used to evaluate the hierarchical structure of biological minerals such as teeth and bone, and has been employed by various researchers to examine the crystalline structures of biological mineral composites [12–14]. Xue et al. used X-ray microdiffraction and TEM to characterize and analyze human tooth structures and found a good correlation between XRD and TEM. They concluded that μXRD is a useful technique for evaluating the crystalline structures of heterogeneous enamel and dentin [15].

Detailed information of the crystalline structure of dental enamel in terms of the percentage of crystallinity [14], dimensions of lattice parameters [16], microstrain of crystallites [13], crystallite orientation [17], and the positions of atoms and occupancies of sites [18] can be obtained using powder XRD. Simmons et al.. studied the distribution of both direction and magnitude of the preferred orientation of enamel crystallites within an entire tooth crown using synchrotron XRD and found a high spatial heterogeneity in both the magnitude and direction of the crystallites orientation [17]. Using XRD analysis, it was also demonstrated that the crystal size of polycrystalline materials affects their mechanical and physical properties [19]. Eimear et al. reported that the size of enamel nanocrystals influences the tooth's optical properties [20] and also determined that the hardness of enamel is mainly regulated by thecarbonate apatite (CAP)crystal size [16].

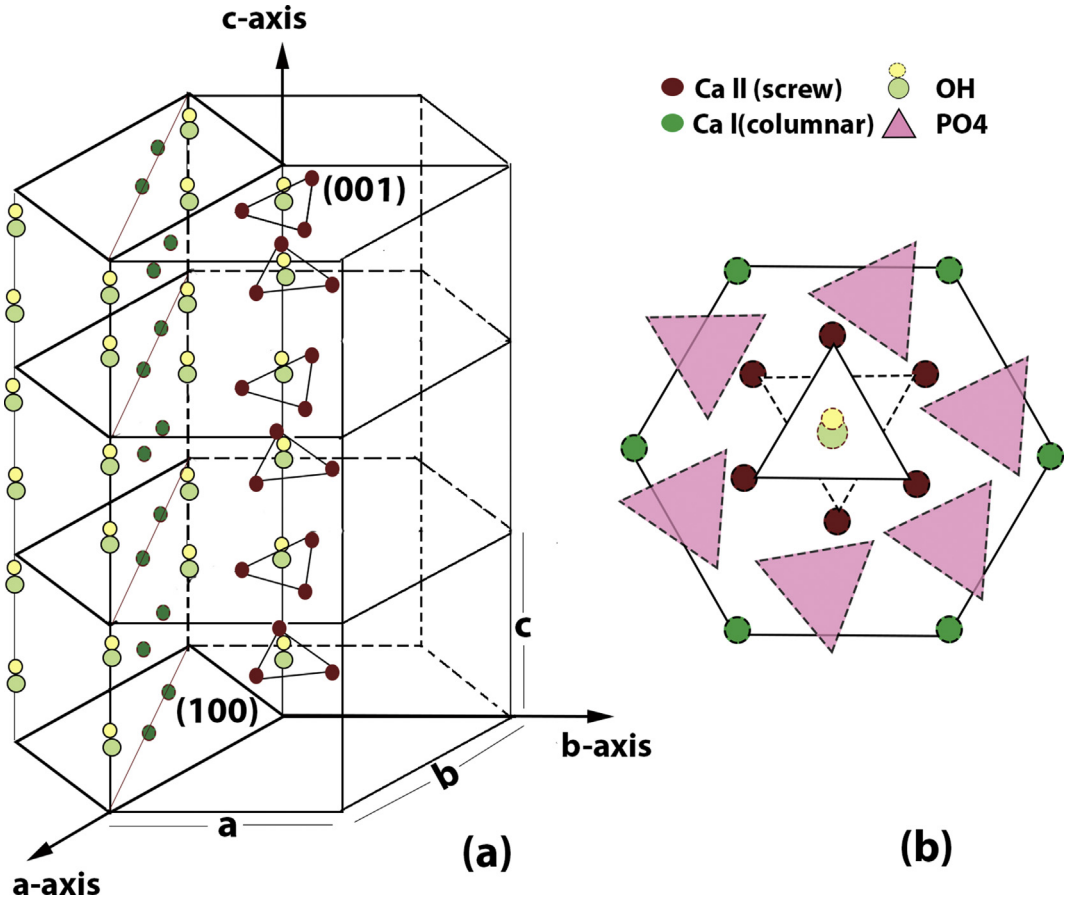

Fig. 2. Schematic of the position of columnar and screw calcium, phosphate ions, and hydroxyl groups on an enamel apatite unit cell. Three Ca^{+2} (Ca II) ions form a triangle centered on the hexad axis. Ca I ions form long columns in apatite structures that are close to phosphate ions: (a) hexagonal system of enamel apatite, direction of lattice parameters, and main lattice planes; (b) relationship and arrangement of calcium and phosphate ions around the monovalent column. The figure derived from Ichijo et al. [6].

To study the crystallographic properties of tooth structures, traditional XRD usually employs powder specimens. However, the powder XRD technique has some constraints that restrict its usage. Specifically, this method is a destructive technique in which the sample must be ground and a certain amount of powder must be obtained to form a valid sample, such that information about small or specified areas may be lost [15]. Thus, some researchers prefer to use tooth sections instead of powdered specimens. Because of the organized order of building crystallites in a bulk material, the obtained XRD pattern may swerve from that of the powder specimen [21], and some acquired crystalline information may be altered.

Accordingly, the aim of the present study was to determine and compare the crystalline structures of powder and bulk human dental enamel using XRD analysis.

2. Materials and methods

2.1. Sample preparation

Analyzed samples were obtained from the buccal surfaces of 60 human noncarious third molars. The specimens were cleaned and stored in 0.5% chloramine solution for a week. After observation under a stereomicroscope, any tooth with white spots, caries, cracks, and/or defected areas was excluded from the study. The crowns of teeth were separated from the root and sectioned in 3 × 5 × 3 mm slices using a low-speed diamond saw (Isomet, Buehler, Lake Bluff, II, USA). The slices were then randomly sorted into two groups: Powder and bulk.

To prepare enamel powders, the enamel was first separated from dentin by creating a crack at the enamel-dentin junction. The enamel tissues were then ground and powdered manually using a mortar and pestle. The prepared powders were sieved to select particle sizes between 30 and 40 μm [22]. Powder XRD measurements-ray powder diffraction measurements were performed on the obtained powder samples using an INEL EQUINOX 2000 diffractometer with Cu-Kα radiation of 1.540598 Å working at 40 mA, 40 kV, and a scan speed of 0.02 s^{-1}. The scan range was taken from 10 to 100°.

The crystalline structures of bulk enamel sections that were less than 3-mm thick were analyzed using an X-ray diffractometer (X'Pert PRO MPD, PANalytical Company, Netherlands) with the same parameters as the powder samples. Finally, the obtained data were analyzed using X'Pert HighScore Plus V3 software.

The main peaks of the XRD patterns as well as the values of the lattice parameters, crystal size, microstrain of crystallites, and entire area under the peaks were considered as the criteria for crystallinity to assess the crystalline structures of powder and bulk samples in this study.

2.2. Lattice parameters

The values of the a and c axes of hexagonal unit cells were calculated from (300) and (002) reflections, respectively, according to the following equation of hexagonal crystalline structures [23]:

$$\frac{1}{d^2}=\frac{4}{3}\left(\frac{h^2+hk+k^2}{a^2}\right)+\frac{l^2}{c^2} \quad (1)$$

where d is the interplanar spacing of the crystal structure, a and c are the a and c axes, respectively and h, k, and l are the Miller indices.

2.3. Crystallite size and lattice strain

The average crystal dimensions of each enamel sample were calculated using Scherrer's equation [24] for the (002), (300), and (211) Bragg peaks.

$$D_{hkl} = K\lambda/\beta_{hkl}\cos\theta \quad (2)$$

where D is the average crystal diameter in the direction perpendicular to the lattice planes, hkl denotes the Miller indices of the analyzed planes, K is the crystallite-shape factor (K = 0.94), λ is the wavelength of the X-rays (~1.540598 Å Cu-Kα radiation), β is the line broadening full width at half the maximum intensity (FWHM) in radians, and θ is the Bragg diffraction angle.

The crystallite size and lattice strain were also calculated using the W–H equation [25]. According to the W–H model, the peak broadening is the sum of broadening derived from the crystallite size and lattice strain, $\beta_t = \beta_1 + \beta_2$. The crystallite size peak broadening can be calculated using Scherrer's equation as follows: $\beta_1 = kK\lambda/d\cos\theta$, where β_1 is the broadening of the peak consequent to the crystallite size. The broadening due to the lattice strain β_2 can be calculated by the following relationship:

$$\beta_2 = C\tan\theta \quad (3)$$

where C is the lattice strain and θ is the Bragg diffraction angle.

Thus, we can estimate the total peak broadening as:

$$\beta_t = C\frac{\sin\theta}{\cos\theta}+\frac{K\lambda}{d\cos\theta} \quad (4)$$

By rearranging (4), we can obtain the following equation:

$$\beta_t\cos\theta = C\sin\theta + \frac{K\lambda}{d} \quad (5)$$

A linear fit is then plotted from the scattered results of the main Bragg peaks with $\sin\theta$ and $\beta\cos\theta$ (in radians) on the x and y axes, respectively. The crystallite size and lattice strain can be estimated from the y intercept and slope of the linear equation ($y = mx + n$) of the plotted line, respectively.

2.4. Crystallinity

The degree of crystallinity of both powder and bulk samples was also quantitatively estimated. To produce precise peak positions and areas, profile fitting was conducted using the pseudo-Voigt profile function, which is a linear combination of Gaussian and Lorentzian components. Then, the percentage of the “sum of net area” to “sum of total area” was measured as the criterion for the degree of crystallinity using PANalytical X'Pert HighScore software [26].

2.5. Statistical analysis

Prior to the statistical analysis, the normality and homogeneity of variances of data were tested using the Kolmogorov–Smirnov and Levene's test, respectively. The data were then analyzed by a parametric independent t-test and nonparametric Mann–Whitney test according to the normal or skewed distribution of data. All statistical analyses were conducted using SPSS 23.0 for Windows at a significance level of 0.05.

3. Results

The XRD patterns for powdered and thinly sectioned enamel are shown in Fig. 3. The spectra indicated that the peak positions of

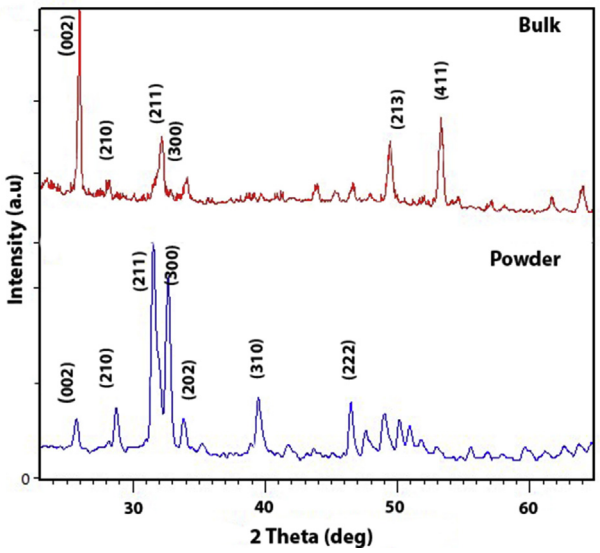

Fig. 3. Representative XRD pattern of powder and bulk tooth enamel in the range of $2\theta = 20–70°$.

Table 1
Lattice parameters of powder and bulk enamel samples

Groups (n = 30)	*a* axis (Å)			*c* axis (Å)		
	mean	SD	*p* value	mean	SD	*p* value
Powder	9.440	0.052	0.78	6.873	0.031	0.8
Bulk	9.444	0.054		6.871	0.011	

Table 2
% Crystallinity of powder and bulk enamel specimens

% Crystallinity			
Groups (n = 30)	mean	SD	*p* value
Powder	49.13	5.21	0.00
Bulk	31.22	4.91	

both groups corresponded to the HAp PDF card number (JCPDF 09-0432).

The figure shows that the peak intensity corresponding to (002) reflection obviously decreased in the powder sample. However, the peak intensities of the (211) and (300) planes were significantly stronger in the powder sample than in the bulk sample. The peak (300) in the bulk sample was nearly merged in the (211) peak. Changes in the intensity of some minor peaks including (213), (411), (310), and (222) could also be seen in the XRD of the powder patterns as compared with the bulk pattern.

Lattice parameters of the bulk and powdered crystallites, calculated according to the equation of hexagonal crystalline structures [23], are presented in Table 1. The data indicated no difference between lattice parameters of sectioned and powdered enamel samples. The independent t-test showed no statistically significant difference between groups in both the *a*- and *c*-axis parameters.

Division of the total area of crystalline peaks by the total area under the diffraction spectra peaks showed significantly higher crystallinity in the powder group than in the bulk group (Table 2). This finding can be attributed to more diffraction peaks in the powder spectra.

The mean crystallite size was measured using both the Scherrer and W–H equations in nanometers. As shown in Table 3, a greater mean crystallite size was obtained in bulk enamels compared to powdered enamels, according to both methods. This difference was statistically significant with both the Scherrer and W–H methods ($p \leq 0.001$).

The microstrain results (in percentage) were obtained from the y intercept of the linear equation of $y = mx + n$ plotted using the W–H method. Because the microstrain results did not follow a normal distribution, we employed the Mann–Whitney test for analysis of the microstrain results of the two groups. The results showed a value nearly twice as high for the microstrain of the powder group as compared to the bulk group. However, this difference was not statistically significant ($p = 0.76$).

A representative Williamson–Hall plot of both powder and bulk groups is shown in Fig. 4.

4. Discussion

Understanding the ultrastructures of natural teeth and the variations in HAp crystallites helps to further understand new concepts regarding caries-prevention methods and novel biomimetic preventive materials. XRD analysis is a powerful method that has been commonly employed to study the ultrastructures of materials [27,28].

Powder XRD is one of the most common methods of XRD, the use of which can help obtain valuable information about constituent phases, average crystallite dimensions, crystallite strains, percentages of crystallinity, and residual stresses of a material [28]. However, achieving an adequate amount of tooth powder required for this method is difficult. Moreover, grinding dental tissues into powder of specific dimensions destroys the tooth structure and leads to the loss of information regarding tooth HAp crystallites [15]. By contrast, in non-destructive XRD methods, the regular arrangement of enamel crystallites produces an anisotropic X-ray intensity distribution, which shows the textured arrangement of enamel crystallites. [10,29]. This regular order of crystallites can be a source of error when evaluating the crystalline structures of materials [29]. Nevertheless, many researchers prefer to employ non-destructive XRD methods considerable information about enamel ultrastructures has been obtained from powder XRD techniques in different studies. The goal of this study was first to determine and then to compare the crystalline structure of dental

Table 3
Crystallite size (nm) and Williamson–Hall lattice strain (%) of groups

Crystal size					Microstrain (%)	
Groups (n = 30)	Scherrer's equation (nm)		Williamson–Hall equation (nm)			
	mean	SD	mean	SD	mean	SD
Powder	28.75	3.40	35.47	8.60	0.0061	0.0086
Bulk	42.20	9.57	47.29	12.92	0.0038	0.0022

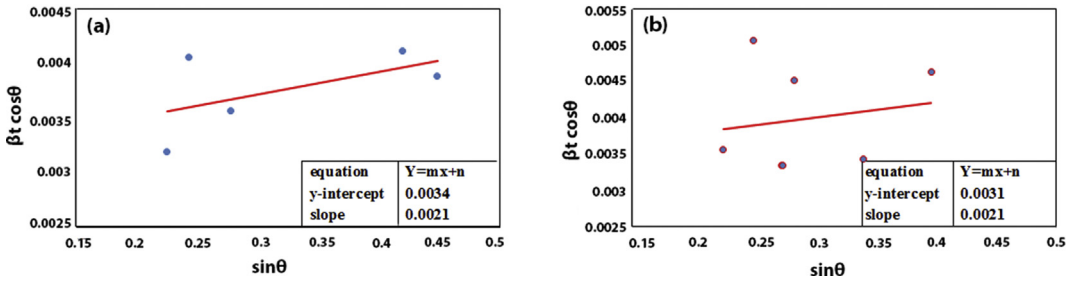

Fig. 4. Representative W–H plot of both (a) bulk and (b) powder groups.

enamel analyses derived from destructive and non-destructive XRD techniques.

Comparison of XRD patterns of bulk and powder samples from Fig. 3 revealed that the intensities of most peaks, including (211), (300), (310), and (222), were stronger than those of bulk samples. By contrast, the (002) peak of the bulk sample had a significantly higher intensity than the powder sample. In the powder sample, because of the random orientation of grains, diverse crystallographic planes could be detected, whereas in the bulk material, the order of crystallites of the material was not as random as that of the powder sample. Thus, the XRD pattern of a bulk material can be different from that of its powder complement. Accordingly, a significantly high peak intensity could be obtained in the XRD patterns of a bulk material from crystallographic plans with preferential alignment [21]. The higher intensity of the (002) plane in the bulk XRD pattern shows that a greater number of (002) planes were perpendicular to the diffraction vector and were involved in reflecting the incident beam. By considering the hexagonal close-packed structure of HAp crystallites of enamel (Fig. 2), we find that the *c* axis of crystallites is perpendicular to (002) planes, which may imply the preferential alignment of crystallites along the *c* axis in bulk enamel [21,30]. Because in this study the percentage of crystallinity was measured by dividing the total area of crystalline peaks by the total area under the diffraction curve, the obtained higher crystallinity of powder samples could be attributed to the greater number of lattice planes being exposed to the incident beam.

Considering the main component of enamel, HAp, the extent and quality of hydroxyapatite lattice imperfection affects the resistance of the teethto fracture [29]. A perfect crystal would infinitely extend in all directions. However, because of the finite size of crystals, no perfect crystal can be found. Any deviation from perfect crystallinity causes peak broadening in a diffraction pattern [31]. Bragg peaks are broadened because of either the crystallite size being smaller than a micrometer or because of nonuniform lattice strains [31,32]. Lattice strain arises from lattice imperfections, and crystallite size is a measure of the sizes of diffracting domains that are aligned coherently [31]. Different sources of strain include dislocations, stacking faults, twinning, grain boundaries, internal stresses, chemical heterogeneities, and point defects [32].

Different methods, including those of Scherrer, W–H the strain–size plot, and Warren-Averbach, have been developed to measure the crystal size and strain of polycrystalline material from XRD data. The Scherrer and Williamson–Hall methods are dependent on both the FWHM values and integral breaths [33]. In this study, we employed both the Scherrer and W–H methods for measuring crystallite size and the W–H method alone to assess lattice strain.

Most studies that measure the crystal sizes of dentin and enamel crystallites have employed Scherrer's equation [16,34–36]. We previously described that peak broadening is produced as a result of both crystallite size and lattice strains. The Scherrer method does not consider the strain-induced width broadening and underestimates the grain size by neglecting the strain broadening. Thus, it is a proper method for strain-free crystallites. Ichijo et al. reported different imperfections, including point defects, line defects, and dislocations in tooth structures. These imperfections can act as a source of strain in the hard-tissue crystalline structures of teeth [37]. Accordingly, the W-Hequation is more suited to determining the crystallite size of the tooth structure because with this method, in addition to the crystallite size peak broadening, the strain-induced peak broadening is considered. Thus, the higher crystallite size value derived from the W–H method as obtained in our study can be attributed to considering strain-induced peak broadening of strain-containing enamel crystallites. The higher crystallite size derived from the W–H method than from the Scherrer method in our results is in agreement with the other studies [38,39].

In this study, the obtained crystallite sizeesof bulk enamels were significantly higher than those of powder samples. It was previously reported that mechanical grinding reduces the particle size and preferred orientation while increasing the lattice strain of the materials [40,41]. During milling, the particle size is reduced to a saturation value and, simultaneously, the lattice strain of the crystal structure increases because of the generation of dislocations and crystal defects. Moreover, in mechanically milled hexagonal close-packed and face-centered cubic structures, different stacking faults have been observed [40]. The results of this study are in agreement with the results of Colaco et al., who reported a higher average crystallite size as well as fewer crystal defects and lower lattice strains in enamel slices as compared to enamel powder samples [35].

In enamel chemistry, different substitutions and compositional structures indicate the values of lattice parameters. Thus, any changes in chemical structures may change the lattice parameters of enamel crystallites. It is known that some anions like fluoride can contract the *a*-axis value, whereas some ions including HPO_4^{2-}, and Cl^- can increase the size of the *a*-axis parameter [4]. Accordingly, any treatment that causes chemical changes in the enamel structure may induce lattice parameter changes. In our study the powdering process of tooth enamel did not induce any chemical changes in enamel crystallites. Thus, the values obtained for the lattice parameters of the powder samples and those of the bulk samples were similar.

5. Conclusion

In this study, it was determined that there is a significant difference between the XRD data of crystalline structures obtained from powder and bulk human dental enamel. Because of this difference, the method of sample preparation should be considered for the studies related to the enamel's crystal structure. Therefore, based on the results of this study, we can achieve more precise scientific investigations and conclusions for tooth enamel structure research when the preparation method for XRD tests is considered.

Ethical statement

1- We declare that this article is entirely original and was checked by PlagScan software. Statements attributed to other studies were cited appropriately,
2- If anyone (reviewers or journal editors) request that we send original (raw) data, we will immediately do so.
3- The study was conducted in vitro. Therefore, we were not required to follow the regulations of animal or human studies.
4- The enamel slabs and powders were obtained from human noncarious third molars, which were extracted for medical purposes after approval from the Human Ethics Committee (reference code: TUMS.REC.1394.301).

Acknowledgments

The authors declare no potential conflicts of interest regarding the publication of this study. This article was part of a larger study supported by the Tehran University of Medical Sciences and Health Services (grant 94-03-69-29375). We are grateful to M. Kaffash and F. Manuchehri for their valuable assistance.

Conflicts of interest

No potential conflicts of interest are reported by the authors.

Appendix A. Supplementary data

Supplementary data to this article can be found online at https://doi.org/10.1016/j.job.2019.06.003.

References

[1] Simmer JP, Fincham AG. Molecular mechanisms of dental enamel formation. Crit Rev Oral Biol Med 1995;6:84–108.
[2] Cui FZ, Ge J. New observations of the hierarchical structure of human enamel, from nanoscale to microscale. J Tissue Eng Regenerat Med 2007;1:185–91.
[3] Palmer LC, Newcomb CJ, Kaltz SR, Spoerke ED, Stupp SI. Biomimetic systems for hydroxyapatite mineralization inspired by bone and enamel. Chem Rev 2008;108:4754–83.
[4] Eanes E. Enamel apatite: chemistry, structure and properties. J Dent Res 1979;58:829–36.
[5] Elliott J, Wilson R, Dowker S. Apatite structures. Adv X Ray Anal 2002;45:172–81.
[6] Ichijo T, Yamashita Y, Terashima T. Observations on the structural features and characteristics of biological apatite crystals. 2. Observation on the ultrastructure of human enamel crystals. Bull Tokyo Med Dent Univ 1992;39:71–80.
[7] Reyes-Gasga J, Martinez-Pineiro EL, Rodriguez-Alvarez G, Tiznado-Orozco GE, Garcia-Garcia R, Bres EF. XRD and FTIR crystallinity indices in sound human tooth enamel and synthetic hydroxyapatite. Mater Sci Eng C Mater Biol Appl 2013;33:4568–74.
[8] Elliott JC. Structure, crystal chemistry and density of enamel apatites. Ciba Found Symp 1997;205:54–67. discussion 72.
[9] Zhan J, Tseng Y-H, Chan JCC, Mou C-Y. Biomimetic formation of hydroxyapatite nanorods by a single-crystal-to-single-crystal transformation. Adv Funct Mater 2005;15:2005–10.
[10] Al-Jawad M, Steuwer A, Kilcoyne SH, Shore RC, Cywinski R, Wood DJ. 2D mapping of texture and lattice parameters of dental enamel. Biomaterials 2007;28:2908–14.
[11] Williams DB, Carter CB. The transmission electron microscope. Transmission electron microscopy. Springer; 1996. p. 3–17.
[12] Raue L, Gersdorff N, Rödiger M, Klein H. New insights in prism orientation within human enamel. Arch Oral Biol 2012;57:271–6.
[13] Kallistová A, Horáček I, Šlouf M, Skála R, Fridrichová M. Mammalian enamel maturation: crystallographic changes prior to tooth eruption. PLoS One 2017;12:e0171424.
[14] Kallistová A, Skála R, Šlouf M, Čejchan P, Matulková I, Horáček I. Enamel apatite crystallinity considerably contributes to mammalian dental adaptations. Sci Rep 2018;8:5544.
[15] Xue J, Zavgorodniy AV, Kennedy BJ, Swain MV, Li W. X-ray microdiffraction, TEM characterization and texture analysis of human dentin and enamel. J Microsc 2013;251:144–53.
[16] Eimar H, Ghadimi E, Marelli B, Vali H, Nazhat SN, Amin WM, et al. Regulation of enamel hardness by its crystallographic dimensions. Acta Biomater 2012;8:3400–10.
[17] Simmons LM, Al-Jawad M, Kilcoyne SH, Wood DJ. Distribution of enamel crystallite orientation through an entire tooth crown studied using synchrotron X-ray diffraction. Eur J Oral Sci 2011;119(Suppl 1):19–24.
[18] Wilson R, Elliott J, Dowker S. Rietveld refinement of the crystallographic structure of human dental enamel apatites. Am Mineral 1999;84:1406–14.
[19] Sriraman KR, Ganesh Sundara Raman S, Seshadri SK. Influence of crystallite size on the hardness and fatigue life of steel samples coated with electrodeposited nanocrystalline Ni–W alloys. Mater Lett 2007;61:715–8.
[20] Eimar H, Marelli B, Nazhat SN, Abi Nader S, Amin WM, Torres J, et al. The role of enamel crystallography on tooth shade. J Dent 2011;39(Suppl 3):e3–10.
[21] Fu J, He C, Xia B, Li Y, Feng Q, Yin Q, et al. c-axis preferential orientation of hydroxyapatite accounts for the high wear resistance of the teeth of black carp (Mylopharyngodon piceus). Sci Rep 2016;6:23509.
[22] Reyes-Gasga J, Martinez-Piñeiro E, Bres E. Crystallographic structure of human tooth enamel by electron microscopy and x-ray diffraction: hexagonal or monoclinic? J Microsc 2012;248:102–9.
[23] Hammond C. The basics of cristallography and diffraction. Hammond C. 2001. Oxford.
[24] Scherrer P. Bestimmung der Grosse und der inneren Struktur von Kolloidteilchen mittels Rontgenstrahlen. In: Alexander LE, editor. X-ray diffraction methods in polymer science; 1918. p. 1969.
[25] Williamson G, Hall W. X-ray line broadening from filed aluminium and wolfram. Acta Metall 1953;1:22–31.
[26] Naghibi S, Faghihi Sani MA, Madaah Hosseini HR. Application of the statistical Taguchi method to optimize X-SiAlON and mullite formation in composite powders prepared by the SRN process. Ceram Int 2014;40:4193–201.
[27] Bunaciu AA, UdriŞTioiu EG, Aboul-Enein HY. X-ray diffraction: instrumentation and applications. Crit Rev Anal Chem 2015;45:289–99.
[28] Tamura N, Gilbert PU. X-ray microdiffraction of biominerals. Methods in enzymology. Elsevier; 2013. p. 501–31.
[29] Reyes-Gasga J, Koudriavtseva O, Herrera-Becerra R, Escobosa A. XRD characterization of crystallinity of human tooth enamel under influence of mechanical grinding. Mater Sci Appl 2015;6:464.
[30] Egan CK, Jacques SD, Di Michiel M, Cai B, Zandbergen MW, Lee PD, et al. Non-invasive imaging of the crystalline structure within a human tooth. Acta Biomater 2013;9:8337–45.
[31] Zak AK, Majid WA, Abrishami ME, Yousefi R. X-ray analysis of ZnO nanoparticles by Williamson–Hall and size–strain plot methods. Solid State Sci 2011;13:251–6.
[32] Ungár T. Microstructural parameters from X-ray diffraction peak broadening. Scripta Mater 2004;51:777–81.
[33] Irfan H, Racik KM, Anand S. Microstructural evaluation of CoAl2O4 nanoparticles by Williamson–Hall and size–strain plot methods. J Asian Ceram Soc 2018;6:54–62.
[34] Leventouri T, Antonakos A, Kyriacou A, Venturelli R, Liarokapis E, Perdikatsis V. Crystal structure studies of human dental apatite as a function of age. Int J Biom 2009;2009:698547.
[35] Colaco MV, Barroso RC, Porto IM, Gerlach RF, Costa FN. Comparison between powder and slices diffraction methods in teeth samples. In: International nuclear atlantic conference - INAC 2011 Belo Horizonte,MG, Brazil, October 24-28, 2011. ASSOCIAÇÃO BRASILEIRA DE ENERGIA NUCLEAR - ABEN; 2011. ISBN: 978-85-99141-04-5.
[36] Xue J, Zhang L, Zou L, Liao Y, Li J, Xiao L, et al. High-resolution X-ray microdiffraction analysis of natural teeth. J Synchrotron Radiat 2008;15:235–8.
[37] Ichijo T, Yamashita Y, Terashima T. Observations on structural features and characteristics of biological apatite crystals. 7. Observation on lattice imperfection of human tooth and bone crystals II. Bull Tokyo Med Dent Univ 1993;40:193–205.
[38] Bindu P, Thomas S. Estimation of lattice strain in ZnO nanoparticles: X-ray peak profile analysis. J Theor Appl Phys 2014;8:123–34.
[39] Weibel A, Bouchet R, Boulc ' F, Knauth P. The big problem of small particles: a comparison of methods for determination of particle size in nanocrystalline anatase powders. Chem Mater 2005;17:2378–85.
[40] Suryanarayana C. Mechanical alloying and milling. Prog Mater Sci 2001;46:1–184.
[41] Snyder JK. Analysis of crystalline phases by x-ray diffraction: effects of sample grinding. University of North Dakota; 1992.